

# Estimating reddening of the continuum and broad-line region of active galactic nuclei: the mean reddening of NGC 5548 and the size of the accretion disc

C. Martin Gaskell<sup>1,\*</sup>, Frances C. Anderson<sup>1,2</sup>, Sufia Á. Birmingham<sup>1,3</sup>,  
Samhita Ghosh<sup>1,4</sup>

<sup>1</sup>*Department of Astronomy and Astrophysics, University of California, Santa Cruz, CA 95064*

<sup>2</sup>*Department of Engineering, Harvey Mudd College, Claremont, CA 91711*

<sup>3</sup>*Department of Astrophysical Sciences Princeton University, Princeton, NJ 08544*

<sup>4</sup>*Department of Mathematics, University of California Berkeley, Berkeley, CA 94720-3840*

2022 August 24

## ABSTRACT

We use seven different methods to estimate broad-line and continuum reddenings of NGC 5548. We investigate two possible reddening curves considered for active galactic nuclei (AGNs): the mean AGN reddening curve of Gaskell & Benker (2007) which is relatively flat in the ultraviolet, and a curve that rises strongly into the ultraviolet like a Small Magellanic Cloud (SMC) reddening curve. We also consider a standard Milky Way curve. Regardless of the curve adopted, we find a total reddening  $\sim 14$  times greater than the small amount of reddening due to dust in the solar neighbourhood. The UV-to-optical ratios rule out a steep SMC-like reddening curve for NGC 5548. The Milky Way and Gaskell & Benker curves give a mean reddening of  $E(B - V) = 0.25 \pm 0.02$ . The four non-hydrogen-line reddening indicators imply that the intrinsic hydrogen line ratios are consistent with Baker-Menzel case B values. The unreddened optical to UV spectral energy distribution is consistent with the predicted distribution for an externally-illuminated accretion disc. The reddening we derive for NGC 5548 is typical of previous estimates for type-1 AGNs. Neglecting internal extinction leads to an underestimate of the luminosity at 1200 Å by a factor of seven. The size scale of the accretion disc has therefore been underestimated by a factor of  $\approx 2.6$ . This is similar to the accretion disc size discrepancy found in the 2013 *AGNSTORM* campaign and thus supports the proposal by Gaskell (2017) that the accretion disc size discrepancy is primarily due to the neglect of reddening.

**Key words:** galaxies: active — galaxies: nuclei — quasars, emission lines — galaxies: ISM — dust, extinction — galaxies: individual: NGC 5548

## 1 INTRODUCTION

Because it affects almost every aspect of our understanding of active galactic nuclei (AGNs), knowing the total reddening of an AGN is crucial. The majority of studies of the spectral energy distributions (SEDs) and broad-line intensities of type-1 thermal AGNs assume that reddening other than by dust in our solar neighbourhood (typically  $E(B - V) < 0.05$  for high Galactic latitude directions) is negligible. On the other hand, other studies have pointed to substantial reddenings in some AGNs ( $E(B - V) \sim 0.2$  and higher – see

Gaskell 2017 for a review). There are two main reasons why many researchers have assumed that internal reddening is low. The first is that there is only a small amount of additional reddening ( $E(B - V) \sim 0.03 - 0.05$ ) associated with the high-velocity outflows seen in broad absorption line quasars (BALQSOs), and the dust associated with the outflows has a reddening curve that rises strongly going into the UV like the reddening curve of the Small Magellanic Cloud (SMC) bar (see Figure 5 of Gaskell, Gill, & Singh 2016). If  $E(B - V) > 0.1$ , and if the SMC-like reddening curve of BALQSOs is applicable to AGNs in general, the SED of AGNs should fall rapidly going into the far UV. This is seen only rarely. The second reason for thinking that the reddening

\* E-mail: mgaskell@ucsc.edu

ing of AGNs is low is that it has long been thought that in the broad-line region (BLR) of AGNs, Lyman  $\alpha$  is suppressed and the  $H\alpha/H\beta$  ratio increased by collisional and radiative transfer effects (e.g., Ferland & Shields 1985; for a review see Gaskell 2017). If this is the case, observed  $Ly\alpha/H\beta$  and  $H\alpha/H\beta$  ratios imply little or no reddening.

To get around the potential problem with the intrinsic ratios of the BLR hydrogen lines we present here a study of seven different reddening indicators in spectra of NGC 5548, the best-studied, radio-quiet thermal AGN. Four of the reddening indicators do not involve hydrogen lines. Over the past four decades the AGN NGC 5548 has been the subject of many large-scale reverberation mapping campaigns from the X-ray region to the IR. In analyzing recent results, Edelson et al. (2015), Mehdipour et al. (2015), Fausnaugh et al. (2016), Kriss et al. (2019), and others follow the widespread practice of assuming that there is negligible internal reddening along our line of sight and they only correct for reddening in the Milky Way. The latter is very small. Schlegel et al. (1998) get  $E(B - V) = 0.020$  for NGC 5548, a value close to the earlier estimate of  $E(B - V) = 0.017$  by Schlafly & Finkbeiner (2011).

In this paper we address five key issues: (1) are the different independent reddening indicators consistent? (2) are the hydrogen line ratios consistent with Case B ratio? (3) what is the appropriate reddening curve for NGC 5548? (4) what is the average reddening of NGC 5548? and (5) can reddening solve the ‘‘accretion-disc-size discrepancy’’ for NGC 5548? We also briefly consider other consequences of the reddening we find.

The organization of the paper is as follows. In Section 2 we discuss the general problem of estimating AGN reddening AGNs and consider three possible reddening curves. In Section 3 we review and discuss four reddening indicators that do not involve hydrogen lines. We give expected theoretical unreddened ratios and discuss the limitations of each indicator. In Section 4 we discuss the use of three hydrogen line ratios as reddening indicators. In section 5 we use the seven methods to derive colour excesses,  $E(\lambda_1 - \lambda_2)$ , between pairs of wavelengths,  $\lambda_1$  and  $\lambda_2$ , for each reddening indicator. In Section 6 we compare the colour excesses  $E(B - V)$  implied by the seven methods using the three reddening curves we consider. In Sections 7 and 8 we discuss the implications of the reddening we find for the UV luminosity and the size of its accretion disc respectively. In Section 9 we briefly discuss various consequences of our results and we end with some suggestions for optimizing future observing campaigns to improve reddening estimates. Our main conclusions are summarized in Section 10.

## 2 ESTIMATING REDDENING OF AGNS

We follow the standard method of estimating reddenings. We take observed ratios of the fluxes,  $[F(\lambda_1)/F(\lambda_2)]_{\text{obs}}$ , at two different wavelengths,  $\lambda_1$  and  $\lambda_2$ , and then make two assumptions. The first is to assume an intrinsic (i.e., unreddened) flux ratio,  $[F(\lambda_1)/F(\lambda_2)]_{\text{int}}$ . If  $\lambda_1 < \lambda_2$ , the colour excess between the two wavelengths is then

$$E(\lambda_1 - \lambda_2) = -2.5 \log \frac{[F(\lambda_1)/F(\lambda_2)]_{\text{obs}}}{[F(\lambda_1)/F(\lambda_2)]_{\text{int}}}. \quad (1)$$

Our second assumption is to adopt a reddening curve to get standard reddenings in terms of  $E(B - V)$ , the colour excess between the Johnson  $B$  and  $V$  photometric bands. With one exception, the reddening indicators we consider are between other pairs of wavelengths. To convert a colour excess,  $E(\lambda_1 - \lambda_2)$ , to an equivalent  $E(B - V)$  one needs a reddening curve,  $A(\lambda)/E(B - V)$ , where  $A(\lambda)$  is the relative extinction in magnitudes at wavelength  $\lambda$ . From the adopted reddening curve one can determine

$$\frac{E(\lambda_1 - \lambda_2)}{E(B - V)} = \left[ \frac{A(\lambda_1)}{E(B - V)} \right] - \left[ \frac{A(\lambda_2)}{E(B - V)} \right], \quad (2)$$

where the quantities in square brackets on the right are the normalized attenuations for the relevant wavelengths. These are read off from the normalized reddening curve being used. One can thus convert  $E(\lambda_1, \lambda_2)$  into  $E(B - V)$ .

### 2.1 Reddening curves

The shape of a reddening curve depends on the composition and size distribution of the grains and on the geometry of the dust region. The choice of curve is relatively unimportant in the optical and IR because curves are fairly similar, but the choice strongly effects the value of  $E(B - V)$  derived from UV-to-optical reddening indicators because there are large differences in reddening curves at short wavelengths. The steeper the reddening curve is in the UV, the lower  $E(B - V)$  is for a given  $E(UV - \text{optical})$ .

Wampler (1968) presciently noted that ‘‘if the dust causing the reddening [of AGNs] is produced in the nuclei of the Seyfert galaxies, there is no reason to believe that it would have the same reddening properties as dust produced in the spiral arms of our Galaxy.’’ Gaskell et al. (2004) discovered from comparing composite spectra of radio-loud AGNs at different orientations that the reddening curve for these AGNs was substantially flatter in the UV than a typical Milky Way curve in the UV. A subsequent independent analysis by Czerny et al. (2004) of large sample of predominantly radio-quiet SDSS AGNs also gave a reddening curve that was flatter than a typical Milky Way curve in the UV. In contrast to these results, Gaskell, Gill, & Singh (2016) have shown that a reddening curve which steeply rises to the far UV, like the reddening curve of the bar of the SMC bar, is an excellent fit to the reddening curve of dust associated with high-velocity outflows from AGNs (the broad absorption lines). Gaskell & Benker (2007) constructed reddening curves for 14 AGNs with near-simultaneous observations from the far UV to long optical wavelengths. These show some variety in the reddening curves, but only one of the 14 AGNs had a steep SMC-like reddening curve.<sup>1</sup>

In this paper we will consider three reddening curves. The first is a typical Milky Way reddening curve, as parametrized by Weingartner & Draine (2001). A Milky Way curve has long been ruled out for the majority of AGNs because they do not show the strong  $\lambda 2175$  dust feature, so we are only including the Milky Way

<sup>1</sup> Sample selection has an important effect. Samples of AGNs selected by having red UV colors will naturally produce more SMC-like reddening curves. This is the case, for example, for the red AGNs considered by Richards et al. (2003).

**Table 1.** Reddening indicators and reddening curves

Method	$\lambda_{\text{short}}$	$\lambda_{\text{long}}$	Intrinsic ratio	$\frac{E(\lambda_1 - \lambda_2)}{E(B - V)}$ Milky Way	$\frac{E(\lambda_1 - \lambda_2)}{E(B - V)}$ Gaskell & Benker	$\frac{E(\lambda_1 - \lambda_2)}{E(B - V)}$ SMC
Ly $\alpha$ /H $\beta$	$\lambda 1216$	$\lambda 4861$	35	6.75	4.90	16.7
O I	$\lambda 1304$	$\lambda 8446$	6.5	7.64	6.75	17.2
$F_{\text{uv}}/F_{\text{opt}}$	$\lambda 1337$	$\lambda 5100$	1.5	5.68	5.03	14.8
He II	$\lambda 1640$	$\lambda 4686$	8.5	3.99	4.26	9.83
$F_B/F_V$	$\lambda 4450$	$\lambda 5510$	1.18	1.00	1.00	1.00
H $\alpha$ /H $\beta$	$\lambda 4861$	$\lambda 6563$	2.8	1.23	1.23	1.20
Pa $\beta$ /H $\beta$	$\lambda 4861$	$1.28 \mu\text{m}$	0.14	2.81	2.76	2.71

curve for comparison. We then consider two reddening curves proposed for AGNs: the mean AGN reddening curve given by Gaskell & Benker (2007), and an SMC-like curve as parametrized by Weingartner & Draine (2001). Gaskell & Benker (2007) only gave their mean AGN curve for wavelengths from Lyman  $\alpha$  to H $\alpha$ , but we consider Paschen  $\beta$  here as well. Since the SMC and Milky Way curves are similar from H $\alpha$  to Pa $\beta$ , we have extended the Gaskell & Benker curve to longer wavelengths by taking the average of the Milky Way and SMC curves. Table 1 summarizes our adopted factors for the three reddening curves for converting  $E(\lambda_1 - \lambda_2)$  to  $E(B - V)$  for the pairs of wavelengths we consider (i.e., the right hand side of Eq. 2)

### 3 NON-HYDROGENIC REDDENING INDICATORS

Because of the long-standing controversy over hydrogen line ratios (see Section 4), we first consider four reddening indicators that do *not* involve hydrogen lines. We discuss some of the limitations of each indicator and questions that have been raised.

#### 3.1 He II lines

Shuder & MacAlpine (1979) pointed out that, in principle, one of the best reddening indicators for the BLR is the He II  $\lambda 1640/\lambda 4686$  line ratio. Because the abundance of helium by number is a tenth that of hydrogen, and because the lines arise from very high energy levels in gas of high ionization, the He II  $\lambda 1640/\lambda 4686$  ratio is expected to be much less sensitive to the collisional-excitation and optical-depth effects which had been suggested to potentially drastically change hydrogen line ratios (MacAlpine 1981). Photoionization models of the high-ionization BLR (MacAlpine 1981; Bottorff et al. 2002) confirm that the He II  $\lambda 1640/\lambda 4686$  ratio is close to a Baker-Menzel case B value. We adopt a theoretical  $\lambda 1640/\lambda 4686$  intensity ratio of  $8.5 \pm 1$  for the high-ionization BLR (see Figures 2e and 3 of Bottorff et al. 2002). The He II  $\lambda 1640/\lambda 4686$  ratio is not expected to vary much with physical conditions because the lines arise from high levels.

Unfortunately, both He II  $\lambda 1640$  and  $\lambda 4686$  are relatively weak, blended lines. This has deterred their use as a reddening indicator. He II  $\lambda 1640$  is blended with O III]  $\lambda 1663$  and the red wing of C IV  $\lambda 1549$ ; He II  $\lambda 4686$  is blended with broad Fe II  $\lambda 4570$  emission that can often be strong enough

to make He II  $\lambda 4686$  unrecognizable. He II  $\lambda 4686$  can also blend with the blue wing of the strong H $\beta$  line. Stellar absorption lines from the host galaxy are a further complication for He II  $\lambda 4686$ . A problem with measuring He II lines (especially  $\lambda 1640$ ) is that higher-ionization lines are progressively broader than lower-ionization lines (Shuder 1982; Mathews & Wampler 1985; Krolik et al. 1991) because the BLR is strongly radially stratified by ionization (see Gaskell 2009). Because of this, He II cannot be de-blended by assuming that a He II line has the same profile as the contaminating lines.

He II arises in the innermost BLR close to the innermost part of the accretion disc. Because it takes 54 eV to doubly ionized helium, most of the ionizing photons needed to produce He II come from close to the Wien cutoff of the spectrum of the accretion disc. This emission from the innermost accretion disc is the most variable part of an AGN's spectrum. He II comes from ten or more times closer to the black hole than other BLR lines studied (see Gaskell 2009 for a review of the structure of the BLR). Because of the combination of the small size of the He<sup>+</sup> emitting region and the rapid, high variability of the relevant ionizing continuum, He II emission is highly variable. For NGC 5548, He II variations lag continuum variations by less than a day (Korista et al. 1995) rather than the many days or weeks for other broad lines. The He II lines can only be used as a reddening indicator if the He II  $\lambda 1640$  and  $\lambda 4686$  observations are near simultaneous. We will propose in Section 5.1 below that the strong variability of He II can be exploited to overcome the line-blending problem and estimate the  $\lambda 1640/\lambda 4686$  ratio.

#### 3.2 O I lines

Netzer & Davidson (1979) proposed that the O I  $\lambda 1304/\lambda 8446$  ratio is another useful reddening indicator since almost every  $\lambda 8446$  transition will be followed directly by a  $\lambda 1304$  transition. The number of  $\lambda 1304$  photons is the same as the number of  $\lambda 8446$  photons but the intensity of the  $\lambda 8446$  line is stronger because a  $\lambda 1304$  photon has more energy than a  $\lambda 8446$  one. This thus gives an O I  $\lambda 1304/\lambda 8446$  intensity ratio of  $8446/1304 = 6.48$ . Kwan & Krolik (1981) and Grandi (1983) noted minor effects that might possibly change the  $\lambda 1304/\lambda 8446$  ratio (see Grandi 1983, section II d). Various factors which might affect the O I  $\lambda 1304/\lambda 8446$  ratio were also discussed by Rodríguez-Ardila et al. (2002) and modelled by Matsuoka et al. (2007). The latter concluded that the

ratio was close to 6.48 for high-column-density clouds with densities and ionization parameters similar to those expected for the BLR. The situation in real BLRs will be even better because observations imply that BLR emission is spread out and highly radially stratified by ionization (Gaskell et al. 2007; Gaskell 2009), rather than coming from high-column-density clouds where each cloud emits all lines. Furthermore, photons will escape from the sides of clouds (see Figure 3 of Gaskell 2017). We therefore expect the unreddened theoretical O I  $\lambda 1304/\lambda 8446$  ratio to be close to 6.48.

Baldwin et al. (1996) suggested that much of what has been assumed to be the O I  $\lambda 1304$  quartet could be the Si II  $\lambda 1307$  doublet and that the latter could dominate in many objects. Matsuoka et al. (2007) propose that typically Si II makes up 50% of the blend. If this is the case, assuming that the observed  $\lambda 1304/\lambda 8446$  ratio is just giving the ratio of the O I lines will result in a major underestimate of the reddening. However, such strong Si II  $\lambda 1307$  is a problem for emission line modelling because photoionization models cannot produce strong Si II  $\lambda 1307$ . (Baldwin et al. 1996 refer to this as “the Si II disaster” – see their Appendix C). We will nevertheless investigate the question of possible Si II contamination in Section 5.2.

### 3.3 Reddening from the shape of the variable optical flux (Chołoniewski method)

Chołoniewski (1981) made the important discovery that if the apparent brightnesses of an AGN in different passbands – for example, the fluxes  $F_B$  and  $F_V$  in the Johnson  $B$  and  $V$  bands – are plotted against each other as *fluxes* rather than as magnitudes, the curvature seen when plotting in magnitudes disappears. He interpreted the resulting straight lines in flux–flux plots<sup>2</sup> as the addition of a non-varying component (mostly starlight of the host galaxy) and a varying AGN component of fixed spectral shape. He further suggested that differences in the slope in flux-variability plots were a consequence of differing reddening in each AGN. Careful observations and analysis by Winkler et al. (1992), Winkler (1997) and Sakata et al. (2010) have shown that the loci in optical flux-variability plots are indeed straight lines. Winkler et al. (1992), Cackett, Horne, & Winkler (2007) and Heard & Gaskell (2022) also show that there is reasonable agreement with other reddening indicators, thus supporting Chołoniewski’s conjecture.

#### 3.3.1 The unreddened optical flux

To estimate  $E(B - V)$  via the Chołoniewski method one needs to know the spectral shape of the variable component of an unreddened AGN. The optical-to-UV emission of a thermal AGN<sup>3</sup> is dominated by thermal emission from the

accretion disc. The outer parts of the disc are externally illuminated by emission just above the disc plane closer to the centre of the disc. This produces a spectrum with a power-law dependence of the flux per unit frequency on the frequency:  $F_\nu \propto \nu^{+1/3}$  (Friedjung 1985)<sup>4</sup>. Heard & Gaskell (2022) show that the distribution of spectral indices of the variable component of the optical-to-near-UV spectra in over 4000 SDSS AGNs is consistent with the unreddened continuum having the expected  $\nu^{+1/3}$  spectrum after allowance for BLR emission. The intrinsic ratio of the unreddened fluxes per unit frequency between two wavelengths of the disc component alone is thus expected to be

$$\left[ \frac{F(\lambda_1)}{F(\lambda_2)} \right]_{\text{int}} = \left[ \frac{\lambda_2}{\lambda_1} \right]^{+1/3}. \quad (3)$$

Strictly speaking, the theoretical ratio given by Eq. 3 only gives the slope in a flux-variability diagram when *monochromatic* fluxes are plotted, such as fluxes obtained from spectra after allowance for line emission. If the method is being used with fluxes found from broad-band filter measurements (as is frequently the case), contamination by variable line emission and bound-free emission associated with the BLR causes the unreddened SED to deviate somewhat from the expected theoretical spectrum for a pure externally-illuminated accretion disc (see Heard & Gaskell 2022). Depending on where variable strong emission lines and bound-free continua fall with respect to filter passbands, the unreddened slope will be more or less than the slope given by Eq. 3. For low-redshift thermal AGNs, only the  $V$  filter does not include any strong contribution from a broad line. The  $R$  filter, for example, is centred on the very strong, broad H $\alpha$  line. This will make the unreddened  $F_V$  vs.  $F_R$  gradient much less (i.e., redder) than the value given by Eq. 3. The  $R$  filter, and especially the  $I$  filter, also include emission from the hot nuclear dust (see Gaskell 2007 and Sakata et al. 2010). At shorter wavelengths, the  $U$  filter has a strong contribution from the BLR emission making up the “small blue bump” (see Figure 4 of Heard & Gaskell 2022). After the  $V$  band, the filter with the least broad-line emission for low-redshift AGNs is the  $B$  filter but this includes the higher-order Balmer lines blending into the Balmer continuum emission of the long wavelength side of the small blue bump. The unreddened  $F_B$  vs.  $F_V$  flux gradient will thus be greater than the value of 1.07 predicted by Eq. 3. Comparing an observed  $F_B$  vs.  $F_V$  gradient with 1.07 therefore gives only a *lower limit* to  $E(B - V)$ . The effect of the broad-line contamination on the  $B$  band is illustrated by the distribution of  $F_B$  vs.  $F_V$  gradients found by Winkler (1997) for a large sample of low-redshift AGNs. Fully 40% of his  $F_B$  vs.  $F_V$  gradients are greater than the 1.07 predicted by Eq. 3.

One can get an empirical estimate of the unreddened  $F_B$  vs.  $F_V$  gradient of a typical low-redshift AGN by considering the bluest variable AGN continua. One cannot simply take the bluest known gradient because extrema are influenced by observational errors. An accurate estimation of the bluest  $(B - V)$  depends on knowing the errors in the gradient esti-

<sup>2</sup> Note that although the standard procedure has been to determine gradients from flux–flux plots, the gradient can also be obtained from root-mean-square spectra.

<sup>3</sup> See Antonucci (2012) for discussion of the division of AGNs into thermal (high accretion rate) and non-thermal (low accretion rate) AGNs.

<sup>4</sup> Coincidentally and confusingly, this is also the better-known theoretical spectrum produced by the outer parts of the standard internally-heated accretion disc of Lynden-Bell (1969).

mates, something beyond the scope of this study. However, the 90th percentile of the  $F_B$  vs.  $F_V$  gradients of the large Winkler (1997) low-redshift sample is 1.18. We will therefore adopt this as the unreddened  $F_B$  vs.  $F_V$  gradient. The 80th percentile of the distribution gives 1.12, which suggests the uncertainty in the assumed unreddened slope is of the order of  $\pm 0.06$ . Assuming an intrinsic slope of 1.18 compared with 1.07 raises an estimate of  $E(B - V)$  by  $\sim 0.11$  magnitudes. Cackett, Horne, & Winkler (2007) noted that the reddenings they got from the Choloniewski method were systematically lower than the reddenings implied by the Balmer decrements. Increasing their reddenings from flux-variability gradients by 0.11 magnitudes, as suggested here, removes this systematic difference.

In addition to using an incorrect unreddened flux gradient, another factor that will give an incorrect reddening is having a scale-factor error in one of both of the fluxes. Whilst the Choloniewski method automatically removes constant additive components, scale factor errors will give an incorrect slope. When converting broad-band magnitudes to fluxes it is therefore important to use the correct conversion factor for each of the photometric filters used to make the observations.

### 3.4 UV-to-optical continuum flux ratio

The ratio of the UV to optical flux is strongly influenced by reddening. Whilst it is well established that there is little if any variability in the intrinsic SED in the *optical* as an AGN varies (see previous section), this is not necessarily expected to be the case for the shortest wavelengths. This is because of two effects. Firstly, as one goes to shorter wavelengths, one eventually approaches the Wien cutoff of emission from the innermost regions of the disc. This causes a flattening of the SED towards shorter wavelengths and a departure from a  $F_\nu \propto \nu^{+1/3}$  power law at short wavelengths. The continuum variability of high-luminosity AGNs (Heard & Gaskell 2022) suggests that there is indeed happening at least for high-luminosity AGNs (see Figure 2 of Heard & Gaskell 2022). The second effect is that, since the heating of the surface of the accretion disc comes from external illumination, geometric effects alone flatten the rise in temperature with decreasing radius as one approaches the disc centre. This too causes a flattening of the SED at very short wavelengths. The extent to which this flattening varies from object to object as a function of parameters such as black hole mass, luminosity and Eddington ratio needs further investigation but the study by Heard & Gaskell (2022) of continuum variability going out to  $\sim 1200\text{\AA}$  indicates that, after allowance for the “small blue bump” and other emission associated with the BLR, the Choloniewski method can be used down to at least  $2200\text{\AA}$ .

Comparing the variability of  $H\beta$  with predictions from variability of the continuum measured at  $5100\text{\AA}$  shows that they are frequent deviations from the predictions (Gaskell et al. 2021). These “anomalies” are on a timescale of  $\sim 40 \pm 20$  days or so (see Figure 4 of Gaskell et al. 2021) and are independent of the continuum level. Since  $H\beta$  is responding to variations in the ionizing flux with wavelengths shorter than  $912\text{\AA}$ , the anomalies in the  $H\beta$  response must correspond to changes in the UV to optical continuum shape. Because of these it is important not only to try to determine

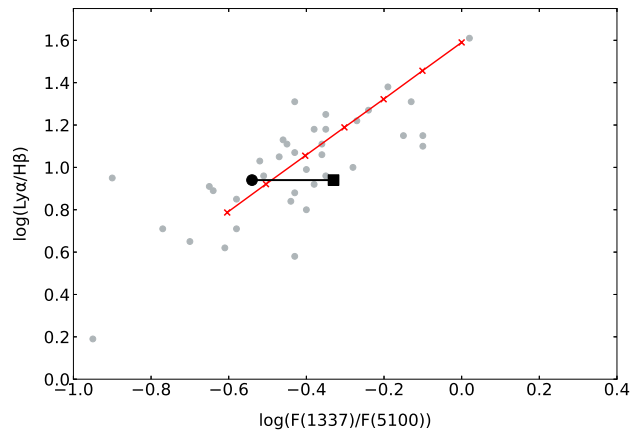


**Figure 1.**  $\text{Ly}\alpha/\text{H}\beta$  ratios versus the ratio of UV to optical continuum fluxes. The gray dots are the AGN measurements reported by Netzer et al. (1995) and Bechtold et al. (1997). The contribution of host galaxy starlight to the optical fluxes has not been allowed for. The filled black circle shows where NGC 5548 falls without removal of the contribution of the host galaxy starlight to the optical flux. The black square is NGC 5548 with the host galaxy starlight removed. The red line is the reddening vector for the Gaskell & Benker (2007) curve (see text) with crosses separated by 0.05 magnitudes in  $E(B - V)$  and starting in the upper right at  $E(B - V) = 0.00$  in the upper right. (Figure adapted from Figure 2 of Gaskell 2017.)

the UV/optical flux ratio from near-simultaneous observations, but also to average over variability.

Despite these expected problems, studies by Netzer et al. (1995) and Bechtold et al. (1997) showed empirically that the  $F_{\lambda 1216}/F_{\lambda 4861}$  continuum flux ratio is correlated with the  $\text{Ly}\alpha/\text{H}\beta$  line flux ratio. Figure 1 shows the combined data sets. Such a correlation is a natural consequence of reddening, but there is no ready explanation of why the intrinsic  $\text{Ly}\alpha/\text{H}\beta$  line ratio might depend on the optical-to-UV spectral slope. This therefore implies that the UV/optical flux ratio can be used at least as an approximate reddening indicator. We assume that the unreddened  $\text{Ly}\alpha/\text{H}\beta$  ratio is close to Case B (see next section) and plot a reddening vector starting at this value. We have adjusted the vector in the continuum flux direction so that it passes through the median of the other AGNs. If we do this, the continuum flux ratio is only slightly less than the value of  $F_{\lambda 1216}/F_{\lambda 4861} = (4861/1216)^{1/3}$  predicted by the extrapolation of the  $F_\nu \propto \nu^{+1/3}$  power-law expected at longer wavelengths. A further cause of uncertainty is that the optical fluxes plotted in Figure 1 are not corrected for the unknown contributions of host galaxy starlight. Correction for these will lower the optical fluxes somewhat and hence increase the UV/optical flux ratio to bring the ratio for the bluest AGNs closer to  $(4861/1216)^{1/3}$ . Because of the uncertainty of the host galaxy starlight contribution, an  $F_{\lambda 1216}/F_{\lambda 4861}$  ratio of 1.2 is not inconsistent with the prediction of 1.5 one gets if the  $F_\nu \propto \nu^{+1/3}$  spectrum of an externally-illuminated accretion disc is extrapolated down to  $\lambda 1300$ . We discuss the size of the host galaxy starlight correction and the location of the ratios for NGC 5548 in Section 5.4 below.

## 4 HYDROGEN LINE RATIOS

We now consider three hydrogen line ratios. The intrinsic hydrogen line ratios have been controversial since the first spectrophotometry of AGNs in the mid-1960s. This controversy, which has been entwined with the AGN reddening question, is reviewed in Gaskell (2017). In the 1960s, low  $\text{Ly}\alpha/\text{H}\beta$  and high  $\text{H}\alpha/\text{H}\beta$  ratios were found which differed from the ratios expected from Case B values of recombination theory (Wampler 1967, 1968). Wampler (1967) noted that reddening of  $E(B - V) \sim 0.2$  could explain the Balmer decrement of Ton 1542. He also estimated the  $\text{Ly}\alpha/\text{H}\alpha$  ratio as  $\approx 2.7$  by comparing high- and low-redshift AGNs (Wampler 1968). This was much less than the Case B prediction. Although reddening offered a solution to the differences from Case B, theoretical calculations by many research groups showed that some of the observational results *could* be explained by radiative transfer and collisional effects instead, but it was difficult to obtain a coherent picture. Gaskell (2017) presented evidence that, after de-reddening, velocity-integrated broad-line hydrogen line ratios in AGNs were consistent with Case B recombination values. He pointed out that optically-thick, one-dimensional-slab radiative transfer models that produce values differing from Case B were unlikely to be relevant to real AGNs because the line radiation would escape from clouds sideways.

### 4.1 $\text{H}\alpha / \text{H}\beta$

For the *narrow*-line region the Balmer decrement,  $\text{H}\alpha/\text{H}\beta$ , is an easy-to-use reddening indicator. The intrinsic ratio is expected to be close to a Menzel & Baker Case B value of 2.7–3.1 (see Table 4.4 of Osterbrock & Ferland 2006). Comparison with other NLR reddening indicators (Gaskell 1982, 1984; Wysota & Gaskell 1988) supports this. However, as noted, for the *broad*-line region there have long been doubts about whether Balmer-line ratios are compatible with simple reddening of case B values. There are two firm observational indications that the intrinsic ratio *does* depend somewhat on physical conditions. Firstly, the Balmer decrement at a given time becomes flatter with increasing gas velocity (Shuder 1982; Crenshaw 1986). Secondly, reverberation mapping shows that the variability-weighted radius of the higher-order Balmer lines is progressively somewhat smaller as one goes up the Balmer series (e.g., Kaspi et al. 2000). These results point to the Balmer decrement getting flatter with increasing density and temperature as is expected closer to the centre of the AGN. This is in agreement with recombination theory which predicts that the Balmer decrement gets flatter with increasing temperature and increasing density. This can be seen in Table 4.4 of Osterbrock & Ferland 2006. Figure 4 of Gaskell (2017) shows the effect for higher densities. Despite these expected and observed effects, the *velocity-integrated* line ratios of the bluest, and presumably least-reddened, AGNs nevertheless imply an intrinsic  $\text{H}\alpha/\text{H}\beta$  ratio of  $\approx 2.8$  for the BLR as a whole (Gaskell 2017). This is close to a Case B value. We will therefore adopt  $\text{H}\alpha/\text{H}\beta = 2.8$  for the velocity-integrated broad lines of NGC 5548.

### 4.2 Lyman $\alpha / \text{H}\beta$

From the correlation between  $\text{Ly}\alpha/\text{H}\beta$  and the UV/optical flux ratio (see Figure 1 and Section 3.4 above) Gaskell (2017) argued empirically that the velocity-integrated  $\text{Ly}\alpha/\text{H}\beta$  flux ratio is close to a Case B value of  $\approx 35$ . Zheng (1992) found that the  $\text{Ly}\alpha/\text{H}\beta$  ratio is higher in the high-velocity wings of the lines. Gaskell (2017) proposed that the Lyman  $\alpha$  enhancement at high velocities is due to continuum fluorescence in the Lyman lines (so-called “Case C” conditions – see Baker, Menzel, & Aller 1938, Chamberlain 1953, and Ferland 1999). Because of this enhancement of Lyman  $\alpha$  in the high-velocity wings, the velocity-integrated intrinsic  $\text{Ly}\alpha/\text{H}\beta$  ratio could be somewhat greater than a Case B value, but for NGC 5548 we will assume a Case B  $\text{Ly}\alpha/\text{H}\beta$  ratio of 35.

### 4.3 Paschen $\beta / \text{H}\beta$

$\text{Pa}\alpha$  and  $\text{Pa}\beta$  are in the near IR and thus comparing them with the Balmer lines samples a different part of the reddening curve than UV to optical ratios. Because  $\text{Pa}\alpha$  and  $\text{Pa}\beta$  arise from higher levels of hydrogen than Lyman  $\alpha$  and the  $\text{H}\alpha$  and have lower transition probabilities, there is less danger of the Paschen lines being affected by collisional and optical-depth effects than  $\text{H}\alpha$ . The intrinsic  $\text{Pa}\beta/\text{H}\beta$  ratio is expected to be  $\approx 0.14$ .

## 5 ESTIMATING THE REDDENING OF NGC 5548

We now use these seven reddening indicators to estimate the reddening of NGC 5548.

### 5.1 He II $\lambda 1640/\lambda 4686$

As noted in Section 3.1, both the  $\lambda 1640$  and  $\lambda 4686$  lines of He II suffer from severe blending with other lines. However, one can use the strong, rapid variability of He II to reduce the effects of contamination of the He II  $\lambda 1640$  and  $\lambda 4686$  lines by other spectral features. Because the ionization potentials of oxygen are only slightly higher than those of carbon for the same stages of ionization, O III]  $\lambda 1663$ , which blends with He II  $\lambda 1640$ , is produced in approximately the same region as C III]  $\lambda 1909$ . Photoionization models show that C III]  $\lambda 1909$  is produced at column densities at order of magnitude higher than He II. The self-shielding model of Gaskell et al. (2007) hence predicts that O III] will be emitted at a radius an order of magnitude larger than He II. This is strongly supported by reverberation-mapping. For NGC 5548, Clavel et al. (1991) get a C III]  $\lambda 1909$  lag of 34 days behind the continuum whilst Korista et al. (1995) get a He II lag of  $< 2$  days. O III]  $\lambda 1663$  therefore cannot follow rapid variability of the ionizing continuum the way He II  $\lambda 1640$  can and does. This is true *a fortiori* for the optical Fe II emission blended with He II  $\lambda 4686$  because Fe II arises in the lowest ionization part of the BLR with an effective radius twice that of  $\text{H}\beta$  (Gaskell et al. 2022). For NGC 5548, Fe II variability will lag the continuum variability by  $\sim 40$  days. Given this much slower response of contaminating lines in the UV and optical, we propose two methods that

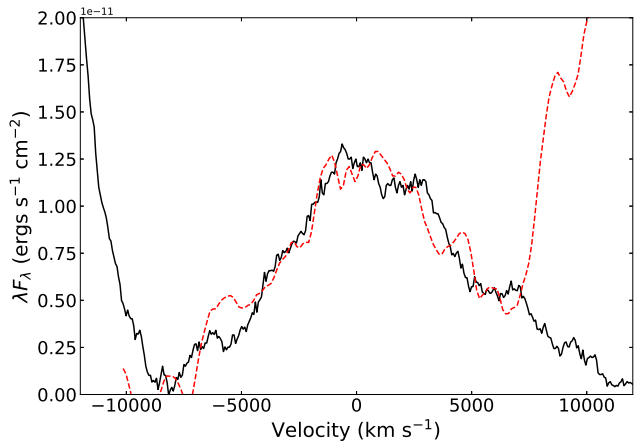


**Figure 2.** Continuum-subtracted UV and optical He II difference spectra between JD 2449128 and JD 2449099. The thick solid line is He II  $\lambda 1640$  and the dashed (red) line is He II  $\lambda 4686$ . The optical spectrum has been multiplied by 4.0 to make the two He II profiles match. The strong UV line bluewards of  $-9000 \text{ km s}^{-1}$  is C IV  $\lambda 1549$  and the strong optical line redwards of  $+7000 \text{ km s}^{-1}$  is H $\beta$ .

exploit the stronger variability of He II for estimating the contamination-free He II  $\lambda 1640/\lambda 4686$  ratio.

### 5.1.1 Difference spectra of He II lines

A ratio of He II  $\lambda 1640/\lambda 4686$  can be found by comparing *difference spectra* between high and low states of He II emission rather than from spectra themselves. Because the lower-ionization lines blending with He II will not vary as much as He II, difference spectra between high and low states will mostly show the highly variable He II line. The variable component of the He II lines can thus readily be identified by subtracting a low state from a high state for which simultaneous optical and UV spectra are available. During the 1993 *International AGN Watch* monitoring campaign (Korista et al. 1995) simultaneous ( $\pm 1$ d) *HST* and optical spectra were obtained on five days. Figure 2 shows continuum-subtracted UV and optical difference spectra for the regions around the He II lines for JD 2449128 and JD 2449099. It can be seen that this has removed all of the O III] and broad optical Fe II emission and that the difference profiles for the two He II lines agree well. The observed ratio is 4. For an intrinsic ratio of 8.5 this gives  $E(\lambda 1640 - \lambda 4686) = 0.82$  magnitudes

### 5.1.2 Line–line variability plots

The other method we propose for exploiting variability to estimate the He II  $\lambda 1640/\lambda 4686$  ratio is to look at the slopes of line flux plots of the different lines. Because  $\lambda 1640$  and  $\lambda 4686$  are from the same ion, *their intensities must be directly proportional*. The slope of the line in the flux-flux plot gives the mean line ratio. We show examples of He II line flux plots in Figures 3 and 4. Just as non-variable host galaxy starlight in the Chóloniewski method does not affect the slope in a plot of varying continuum fluxes, so contaminating non-variable line emission does not affect the slope in a plot of varying line fluxes. Contamination simply produces a constant

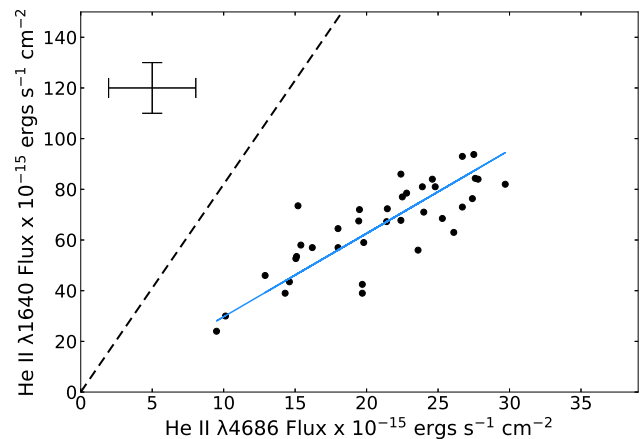


**Figure 3.** Near-simultaneous He II  $\lambda 1640$  vs He II  $\lambda 4686$  fluxes from the 1988-1989 *International AGN Watch* campaign. The  $\lambda 1640$  measurements are the SIPS extracted fluxes from Clavel et al. (1991) and have not had O III  $\lambda 1663$  emission removed. The He II  $\lambda 4686$  has not had Fe II emission removed. The dashed line is a theoretical He II  $\lambda 1640/\lambda 4686$  ratio of 8.5 and the solid (blue) line is an OLS-bisector fit to the data. The He II  $\lambda 4686$  fluxes have been reduced by  $10 \times 10^{-15} \text{ ergs s}^{-1} \text{ cm}^{-2}$  so that this line goes through the origin.

offset. One caveat is necessary though: whilst constant or nearly constant contamination cancels out, systematic scale factor errors in measuring one or both of the lines will not. A scale factor error in one or both fluxes will modify the slope and change the estimated of the line ratio.

Clavel et al. (1991) and Dietrich et al. (1993) give intensities of He II  $\lambda 1640$  and  $\lambda 4686$  respectively for the 1988-1989 *International AGN Watch* NGC 5548 campaign. The published measurements include contamination from other lines which have not been removed. In Figure 3 we show He II  $\lambda 1640$  and  $\lambda 4686$  intensities observed within  $\pm 2$  days.<sup>5</sup> The expected intrinsic unreddened He II  $\lambda 1640/\text{He II } \lambda 4686$  ratio of 8.5 is indicated by the diagonal dashed line. Since quantities plotted in Figure 3 and Figure 4 have errors in both axes, the fits are the ordinary least squares bisector (OLS bisector) advocated by Isobe (1990). For display purposes, to emphasize that what matters is the slope, we have slightly reduced the He II  $\lambda 4686$  fluxes by  $10 \times 10^{-15} \text{ ergs s}^{-1} \text{ cm}^{-2}$  to make the OLS-bisector line pass through the origin. The offset is unimportant; what matters is the slope. The slope of the OLS-bisector gives an observed mean  $\lambda 1640/\lambda 4686$  intensity ratio of  $3.29 \pm 0.12$ . Comparison with the expected intrinsic ratio of  $8.5 \pm 1$  gives a mean  $E(\lambda 1640 - \lambda 4686)$  of  $1.03 \pm 0.19$  magnitudes. The estimated error includes the statistical error in the OLS-bisector slope and the estimated uncertainty in the intrinsic ratio (see Bottorff et al. 2002).

Near-simultaneous He II  $\lambda 1640$  and  $\lambda 4686$  fluxes have also been reported from the 2013 *AGNSTORM* campaign by De Rosa et al. (2015) and Pei et al. (2017) respectively. The uncorrected values as reported are shown as the open circles in Figure 4. Taken at face value these straddle the

<sup>5</sup> Clavel et al. (1991) give fluxes measured with two different extraction routines. We used the fluxes found from the SIPS extraction since they give better consistency between closely-spaced observations.

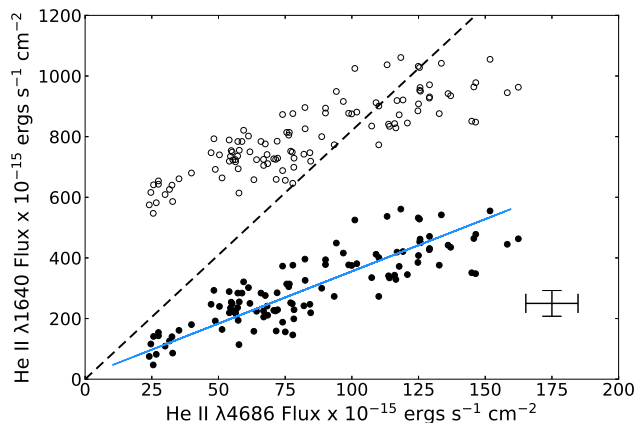


**Figure 4.** Near simultaneous He II  $\lambda 1640$  vs He II  $\lambda 16486$  fluxes from the 2013 *AGNSTORM* campaign. As in Figure 3, the dashed line is a theoretical He II  $\lambda 1640/\lambda 16486$  ratio of 8.5. The reported fluxes are shown as open circles. The solid circles are the result of subtracting  $500 \times 10^{-15} \text{ ergs s}^{-1} \text{ cm}^{-2}$  from the reported He II  $\lambda 1640$  fluxes (see text). The solid (blue) line is an OLS-bisector fit to the shifted data.

theoretical ratio and this could be taken as evidence for no reddening. However, whilst Pei et al. (2017) subtracted out broad optical Fe II emission from He II  $\lambda 4686$ , De Rosa et al. (2015) did not subtract out the substantial O III]  $\lambda 1663$  contribution from He II  $\lambda 1640$ . As explained above O III]  $\lambda 1663$  will be much less variable than He II and will not follow rapid variations of the continuum the way He II does. For display purposes, to again emphasize that what matters is the slope, we have subtracted off a constant flux of  $500 \times 10^{-15} \text{ ergs s}^{-1} \text{ cm}^{-2}$  from the reported He II  $\lambda 1640$  fluxes to make the OLS-bisector line go through the origin. These points are shown as filled circles in Figure 4. Again, the subtraction of a constant has no effect on our reddening estimate which depends only on the slope of the line. The slope of the OLS-bisector fit gives a mean He II  $\lambda 1640/\lambda 16486$  ratio of  $3.44 \pm 0.055$  and hence  $E(\lambda 1640 - \lambda 4686)$  of  $0.98 \pm 0.24$ . Our method thus gives a similar mean reddening for the 2013 *AGNSTORM* campaign as for the 1988–1989 observing campaign even though the He II flux levels were higher in 2013.

In summary, our two different methods of estimating the reddening of NGC 5548 from the He II lines for observing campaigns in three different years are consistent with an unweighted mean  $E(\lambda 1640 - \lambda 4686) \approx 0.94 \pm 0.10$  magnitudes.

## 5.2 O I $\lambda 1304/\lambda 8446$

Figure 5 shows the average O I  $\lambda 1304$  profile for NGC 5548 during the 1993 *HST* monitoring. The two narrow absorption lines in the O I profile (see Fig. 4b of Korista et al. 1995) have been removed, the continuum subtracted, and the spectrum smoothed by a boxcar of half width  $1.75 \text{ \AA}$ . A smoothed H $\beta$  profile taken from the simultaneous optical monitoring of Korista et al. (1995) is shown for comparison. This has been scaled by a factor of 0.22. Grandi (1980) showed that for NGC 4151, O I  $\lambda 8446$  has the same profile as broad H $\alpha$  implying that it comes only from the BLR. It can be seen in Figure 5 that the O I  $\lambda 1304$  profile agrees well with

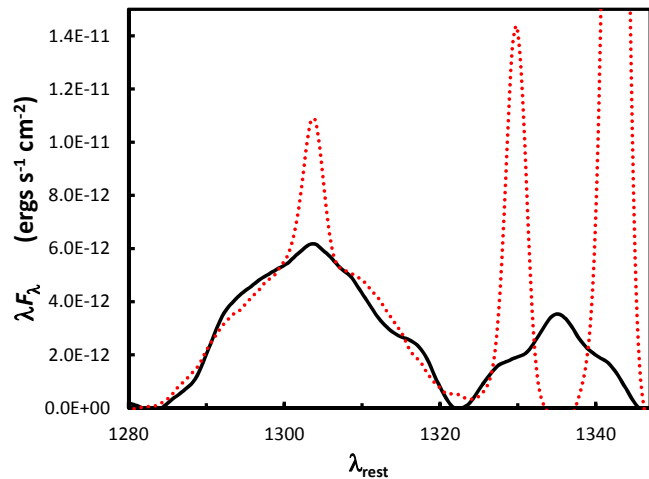


**Figure 5.** A continuum subtracted and smoothed average *HST* spectrum (solid black line) from the 1993 *International AGN Watch* campaign showing the region of O I  $\lambda 1304$  and C II  $\lambda 1335$  emission with narrow absorption lines removed. The dotted (red) line shows a smoothed blueshifted H $\beta$  profile scaled by a factor of 0.22 to O I  $\lambda 1304$ . Note that neither the narrow-line region contribution to H $\beta$  nor the [O III]  $\lambda 4959 \lambda 5007$  lines have been removed.

the broad H $\beta$  profile and clearly lacks a narrow-line region (NLR) contribution. This agreement with the H $\beta$  profile is important because there is no sign of Si II  $\lambda 1307$  emission in the red wing of  $\lambda 1304$ . The weaker line on the right-hand side of Figure 5 is the C II]  $\lambda 1335$  line. Thus, contrary to some suggestions (see Section 3.2), Si II is not a significant contributor to the  $\lambda 1304$  blend in NGC 5548.

To our knowledge, O I  $\lambda 8446$  was not observed during the *HST* monitoring but it has been observed at other times. Landt et al. (2008) give average fluxes for O I  $\lambda 8446$  and H $\beta$  from high-quality spectra obtained on three nights in May 2004, January 2006, and June 2006. These give an O I  $\lambda 8446/\text{H}\beta$  ratio of  $= 0.16$ . Earlier but lower-quality observations of Grandi (1980) gave a similar ratio of 0.18. The relative strength of O I  $\lambda 8446$  compared with H $\beta$  in NGC 5548 is very close to the median relative strength in other AGNs (see Table 1 of Grandi 1980). The O I  $\lambda 8446/\text{H}\beta$  ratio of Landt et al. (2008) and the O I  $\lambda 1304/\text{H}\beta$  ratio during the 1993 monitoring (see Figure 5) give an O I  $\lambda 1304/\lambda 8446$  ratio of  $1.375 \pm 0.08$ . This gives  $E(\lambda 1304 - \lambda 8446) = 1.68 \pm 0.13$  magnitudes.

## 5.3 Optical continuum colour (Chołowiecki method)

Cackett, Horne, & Winkler (2007) get a total reddening of  $E(B - V) = 0.18$  by applying the Chołowiecki method to the 2003 – 2004 photometry of Sergeev et al. (2005) and assuming that the unreddened colour of the variable component is given by a  $F_\nu \propto \nu^{+1/3}$  power law. Similarly, Sakata et al. (2010), from their photometry obtained over the period 2001 – 2007, get  $E(B - V) = 0.13$ .

However, as discussed in Section 3.3.1, because of the higher-order Balmer lines and Balmer continuum in the *B* filter, the unreddened slope in an  $F_B$  vs.  $F_V$  plot will *not* be 1.07 as predicted by Eq. 3. The Cackett, Horne, & Winkler

(2007) and Sakata et al. (2010) reddening estimates are thus lower limits. Using an unreddened gradient of 1.18 instead gives  $E(B - V) \approx 0.26 \pm 0.06$ .

#### 5.4 Reddening from the UV to optical spectral slope

The published UV/optical flux ratios plotted as grey circles in Figure 1 do not include allowance for the uncertain contribution of the host galaxy starlight to the optical continuum flux. For NGC 5548 the starlight contribution to the optical flux *is* known (Bentz et al. 2013). We therefore plotted NGC 5548 in Figure 1 twice, once using the uncorrected optical flux (the filled circle) to match the uncorrected ratios for the other AGNs, and once with the starlight subtracted (the filled square). We have taken average values of the two ratios from Clavel et al. (1991) and Peterson et al. (1991) from the 1988-1989 *International AGN Watch* campaign. The uncertainty in the starlight correction for the AGNs in general is the main uncertainty in using the UV/optical continuum ratio to estimate reddenings. The separation between the two NGC 5548 points in Figure 1 gives an indication of the errors. From Figure 1,  $E(1337 - 5100) = 1.09 \pm 0.26$  where the uncertainty is the uncertainty in the host galaxy starlight subtraction. It is interesting that if the points for the other AGNs (the grey circles) are shifted to the right because of an approximately similar starlight correction as for NGC 5548, the start of the reddening vector is at  $\log F_{1337}/F_{5100} \sim 0.2$  which is the ratio predicted if an  $F_\nu \propto \nu^{1/3}$  spectrum continues to  $\sim 1300$ .

#### 5.5 Lyman $\alpha$ / H $\beta$

Figure 1 shows the mean ratio of Ly $\alpha$ /H $\beta$  using average values from Clavel et al. (1991) and Peterson et al. (1991) the 1988-1989 *International AGN Watch* campaign, that had similar or the same Julian Dates. The average is 8.75. The average error for individual ratios is  $\pm 0.37$ . This corresponds to  $E(Ly\alpha - H\beta) = 1.50 \pm 0.06$ .

#### 5.6 The Balmer decrement

In the optical, the emphasis of the major multi-wavelength NGC 5548 reverberation mapping campaigns has been on H $\beta$  (Peterson et al. 1991, 1992; Korista et al. 1995). Nevertheless, many H $\alpha$  flux measurements are also available (Dietrich et al. 1993). The average H $\alpha$ /H $\beta$  ratio is 3.70 for the 1988-1989 *International AGN Watch* campaign. For an intrinsic ratio of 2.8 this gives  $E(H\alpha - H\beta) = 0.30$  during the campaign. If we adopt an uncertainty in the intrinsic ratio of  $\pm 0.1$ , the error in  $E(H\alpha - H\beta)$  due to this is  $\pm 0.04$ . This does not include probable systematic errors in the measurement of the line ratio.

#### 5.7 Paschen $\beta$ / H $\beta$

From optical and IR observations made in 2004 and 2006 Landt et al. (2008) get a Pa $\beta$  flux of  $1.63 \times 10^{-13}$  ergs s $^{-1}$  cm $^{-2}$  and a H $\beta$  flux of  $3.92 \times 10^{-13}$  ergs s $^{-1}$  cm $^{-2}$ . These give a Pa $\beta$ /H $\beta$  ratio of  $0.42 \pm 0.6$ . These observations were not

simultaneous. Also they were made well outside the times of the UV-optical monitoring campaigns so there is a possibility that the reddening changed, but we include these observations of the Pa $\beta$ /H $\beta$  here because they provide additional evidence for large internal extinction in NGC 5548 consistent with other reddening indicators.

## 6 RESULTS FOR DIFFERENT REDDENING CURVES

In Table 2 we summarize our reddening estimates for the seven indicators and the three reddening curves. As in Table 1, we have ordered the rows by increasing average wavelength of the indicators. Several things are immediately apparent from Table 2.

1. All reddening estimates give reddenings that are *far* greater than the small  $E(B - V) = 0.018$  reddening due to dust in the solar neighbourhood. This is true for *each* of the reddening curves considered.
2. The derived *mean* reddening does not depend strongly on the choice of reddening curve.
3. The SMC reddening curve produces  $E(B - V)$  estimates from the UV that are incompatible with estimates from longer wavelength reddening indicators.
4. For the Gaskell & Benker and the Milky Way reddening curves, the dispersion of the individual reddening estimates about the mean is only slightly larger than the errors in the individual estimates.
5. For the Gaskell & Benker and the Milky Way reddening curves, the hydrogen-line reddening indicators give similar reddenings to the non-hydrogen-line indicators.

Additional support for the Gaskell & Benker (2007) reddening curve being appropriate for NGC 5548 is that comparison of the SED of NGC 5548 with a bluer AGN, such as 3C 273, gives a reddening curve similar to the Gaskell & Benker curve (see Figure 5 of Gaskell et al. 2007).

## 7 THE LUMINOSITY OF NGC 5548

It has long been realized (Wampler 1968) that if there is substantial reddening of the continuum of AGNs, then the UV luminosity will be much higher. Because we are using reddening indicators that go quite far into the UV and are hence measuring the selective extinction between the optical and the UV directly, the total extinction in the UV is well determined and this does *not* depend on the choice of reddening curve adopted. For example, if we take the reddening implied by the O I lines (see Table 2), the Milky Way, Gaskell & Benker. and SMC reddening curves give very similar attenuations at  $\lambda 1200$  of factors of eight, seven, and seven respectively. We can thus conclude that the real luminosity at  $\lambda 1200$  is around a factor of seven greater than observed. Since the reddening curve is probably flat at shorter wavelengths, this means that the bolometric luminosity is also a factor of seven greater than observed.

**Table 2.** Reddening estimates for NGC 5548

Feature(s)	$\lambda_{\text{short}}$	$\lambda_{\text{long}}$	$E(B - V)$ Milky Way	$E(B - V)$ Gaskell & Benker	$E(B - V)$ SMC
Ly $\alpha$ /H $\beta$	$\lambda 1216$	$\lambda 4861$	$0.22 \pm 0.02$	$0.31 \pm 0.03$	$0.09 \pm 0.01$
O I	$\lambda 1304$	$\lambda 8446$	$0.22 \pm 0.03$	$0.25 \pm 0.03$	$0.10 \pm 0.01$
$F_{\lambda 1337}/F_{\lambda 5100}$	$\lambda 1350$	$\lambda 5100$	$0.19 \pm 0.05$	$0.22 \pm 0.05$	$0.07 \pm 0.02$
He II	$\lambda 1640$	$\lambda 4686$	$0.25 \pm 0.02$	$0.24 \pm 0.02$	$0.10 \pm 0.01$
$F_B/F_V$	$\lambda 4400$	$\lambda 5500$	$0.26 \pm 0.06$	$0.26 \pm 0.06$	$0.26 \pm 0.06$
H $\alpha$ /H $\beta$	$\lambda 4861$	$\lambda 6563$	$0.27 \pm 0.03$	$0.27 \pm 0.03$	$0.28 \pm 0.03$
Pa $\beta$ /H $\beta$	$\lambda 4861$	$1.282 \mu\text{m}$	$0.25 \pm 0.12$	$0.25 \pm 0.12$	$0.26 \pm 0.12$
Mean			$0.24 \pm 0.01$	$0.26 \pm 0.01$	$0.17 \pm 0.04$

## 8 THE SIZE OF THE ACCRETION DISC

Because they are so physically thick, accretion discs in AGNs are also optically thick. Accretion disks have similar temperature structures. Except at the very shortest wavelengths, the luminosity of an accretion disc at a given wavelength depends on its surface area and hence on the square of the effective radius. This readily permits one to calculate what the size of the region emitting a given wavelength will be. Continuum reverberation mapping of 14 AGNs by Sergeev et al. (2005) indicated that the sizes of AGN accretion discs were larger than predicted. Using the very different technique of microlensing, Pooley et al. (2006, 2007) found that the inferred sizes of the accretion discs in 10 AGNs were also too large. This is referred to as the “accretion disc size problem”. If it is a real discrepancy, it means that something is seriously wrong with our standard optically-thick accretion disc model for AGNs.

Sergeev et al. (2005) pointed out that the accretion disc size discrepancy could be solved if the luminosities of the AGNs had simply been underestimated. Gaskell (2017) proposed that this was indeed the solution to the disc-size problem and that the luminosities of AGNs were being underestimated by an order of magnitude by neglecting internal reddening. We can quantitatively test this with NGC 5548. For NGC 5548, Edelson et al. (2015) find the size of the accretion disc to be 2.5 times larger than predicted (see their section 4.1). This is similar to the typical size discrepancy in micro-lensed AGNs and other reverberation-mapped AGNs (see Figure 6 of Edelson et al. 2015).

The bulk of the luminosity of a thermal AGN such as NGC 5548 comes out at wavelengths shorter than the  $\lambda 1200$  (see Figure 2 of Gaskell 2008). Since including a correction for internal reddening makes the luminosity of NGC 5548  $\approx 7$  times greater (see previous section), this makes the size of the accretion disc  $\sqrt{7} = 2.6$  times bigger. This is thus in good agreement with the larger disc size found by Edelson et al. (2015) and hence supports the hypothesis that the disc-size problem is simply due to the neglect of internal reddening.

## 9 DISCUSSION

### 9.1 Hydrogen line ratios

An important point is that *the seven reddening indicators we consider here give consistent reddening values for NGC 5548*. Although there can be practical problems in

determining the quantities going into each individual indicator, and although in some cases the observations were not simultaneous, the agreement in reddening estimates in Table 2 shows that, contrary to previous concerns, there are no major problems with the fundamental intrinsic ratios for these indicators. In particular, this includes the hydrogen lines. We can see from Table 2 that the mean reddening from the three hydrogen line ratios is the same as the mean from the four non-hydrogenic indicators. We thus conclude that what has long been referred to as “the hydrogen-line problem” (Lyman  $\alpha$  being too weak relative to the Balmer lines, and the Balmer decrement being too steep) is not a real problem; it is just a consequence of greatly underestimating the reddening. The same goes for the so-called “Balmer line crisis” (the Balmer lines being too strong relative to the UV lines). The hydrogen line ratios are close to their Case B values. Gaskell (2017) argues that the reason for this that real BLR clouds are unlike clouds modelled in photoionization codes. The latter are high-column-density clouds which emit only out of the front of the cloud (towards the source of ionizing radiation) or out of the back. Real BLR clouds have lower column densities and readily emit sideways (see Figure 3 of Gaskell 2017). This means that optical depths are relatively small.

### 9.2 Reprocessing by dust

Energy absorbed by dust from the far UV (FUV) where AGN SEDs peak has to be re-radiated by the dust. This issue has been addressed by Carleton et al. (1987) who considered the overall SEDs of AGNs from hard X-rays to the far red and considered similar reddenings to what we find for NGC 5548. Their Figure 8 is particularly useful. It shows SEDs plotted on a linear  $\nu F_\nu$  scale against  $\log \nu$ , a plot which has the virtue that areas under curves represent energy. From their comparison of the SEDs of AGNs with low reddening (their Class A) with the SEDs of AGNs with reddenings similar to NGC 5548 (their Class B), it can readily be appreciated that the energy lost in the UV in Class B objects compared with Class A objects is reradiated in the IR from 3 – 100  $\mu\text{m}$ . There is thus no energetics problem with having large reddenings of AGNs.

### 9.3 Variable reddening?

If the main factor determining the H $\alpha$ /H $\beta$  ratio is the reddening – as we are advocating here – then changes in the

ratio imply changes in the reddening. This was proposed by Goodrich (1989) as a cause of what are now referred to as “changing-look” AGNs. In the present paper we are focusing on validating reddening indicators and estimating a mean reddening of NGC 5548. We will therefore defer discussion of evidence for variable reddening for the future. We note, however, that Shapovalova et al. (2004) present evidence for  $H\alpha/H\beta$  varying in NGC 5548 both over time and with velocity. Gaskell & Harrington (2018) show this is consistent with variable partial obscuration of the BLR – something supported by absorption line and X-ray variability. Given the possibility of variations in the reddening, the mean reddening we find here might not be applicable for other other years.

#### 9.4 The broad-line region energy budget

Wampler (1968) remarked that “if the continuum is not reddened ... extrapolation of the visual continuum into the ultraviolet indicates that in this case there would be insufficient ultraviolet quanta to ionize the gas.” MacAlpine (1981) showed that there was a severe AGN “energy-budget” problem because observed continua needed an impossible covering factor of  $\Omega/4\pi \gtrsim 9$  to match observed He II  $\lambda 4686$  equivalent widths (see MacAlpine 2003 for a review). Gaskell et al. (2007) examined the energy-budget problem for NGC 5548 for other broad lines and concluded that the problem could only be solved by with significant internal reddening. The reddening we find here is consistent with what the modelling of Gaskell et al. (2007) showed was needed. A very low reddening correcting, such as using only the  $E(B - V) \sim 0.02$  due to Galactic reddening alone, fails to give enough ionizing photons to reproduce the observed broad emission lines in an AGN like NGC 5548.

#### 9.5 Black hole masses

The estimated mass of the black hole in NGC 5548 and, by extension, the masses of other black holes, are not affected by reddening. The mass of the NGC 5548 black hole is estimated using the square of the full width at half maximum (FWHM) of lines times an effective size,  $R$ , which is determined by reverberation mapping, divided by the gravitational constant, and then multiplied by a factor,  $f$ , that depends on the geometry and kinematics of the BLR. The factor  $f$  is calibrated against black holes whose masses have been determined from spatially-resolved stellar dynamics. None of this involves depends on the luminosity of the AGN.

Dibai (1977) proposed estimating black hole masses by estimating  $R$  from the optical luminosity,  $L_{opt}$ , and assuming that  $R = const \times L^\alpha$ . The scale factor and the slope,  $\alpha$ , of the power law of this relationship are calibrated against reverberation-mapped AGNs. A systematic increase in the optical luminosity of AGNs after correcting for reddening merely changes the constant of proportionality. Masses are not systematically increased. Note that it should be possible to improve the  $R - L$  relationship somewhat by allowing for the reddening of individual AGNs.

#### 9.6 Bolometric corrections and Eddington ratios

In the absence of extensive multi-wavelength observations, bolometric luminosities of AGNs are estimated by multiplying a monochromatic luminosity in the optical or UV by a bolometric correction factor. Substantial reddening of AGNs means that the luminosity in the far UV has been underestimated (see above) and hence that bolometric corrections have been systematically underestimated by a significant factor. Higher bolometric corrections in turn increase estimates of Eddington ratios.

The energy lost at shorter wavelengths because of absorption by dust reappears in the infra-red (see Section 9.3). In principle, therefore, a bolometric luminosity based on idealized observations of the *entire* electromagnetic spectrum including the IR will not be affected by absorption. The practical difficulty is in separating out emission in the mid- and far-IR from dust heated by the AGN from emission from dust dust heated by stars. Recognition of the importance of absorption at shorter wavelengths means that less of the mid-IR is due to heating by stars.

#### 9.7 The Sołtan argument

Lynden-Bell (1969) pointed out that there should be super-massive black holes in every massive galaxy. Sołtan (1982) argued that the present-day masses of these black holes had to be consistent with the energy radiated by accretion onto the black holes over the history of the universe. Although this argument is conceptually simple, obtaining the appropriate numbers is complicated. In a detailed study of the Sołtan argument Marconi et al. (2004) find that an average Eddington ratio of 50% is needed (see their Figure 7). This favours higher Eddington ratios and supports the larger bolometric corrections implied by reddening corrections such as what we find for NGC 5548.

#### 9.8 Determining the reddening of AGNs

We have shown that the reddening of NGC 5548, the best-studied type-1 thermal AGN, is substantial. As far as line and continuum ratios go, NGC 5548 is quite typical. so the reddening of most thermal AGNs must also be substantial. Reddening corrections *must* therefore be applied to an AGN first before trying to model SEDs. With only slight modifications to observing campaigns, reddenings can be reliably determined. The modifications are:

- (1) Observe  $H\alpha$  as well as  $H\beta$
- (2) Observe a broad enough wavelength region of the optical spectrum to be able to use the Choloniewski method.
- (3) If the observations include the UV, get simultaneous He II  $\lambda 1640$  and  $\lambda 1640$  observations for at least a relatively high and relatively low state.
- (4) Again, if observing in the UV, Obtain a red spectrum including O I  $\lambda 8446$
- (5) If possible, get a near-IR spectrum including Pa $\beta$

Broad-band optical monitoring can also provide an additional reddening indicator using the Choloniewski method.

## 10 CONCLUSIONS

Our conclusions are as follows:

- (1) We have shown two methods by which reddenings can be obtained from He II lines: either by looking at optical and UV difference spectra, or by looking at the slope of the relationship between He II  $\lambda 1640$  and  $\lambda 1640$  fluxes as they vary.
- (2) Si II contamination of the O I  $\lambda 1304$  is negligible.
- (3) Seven separate reddening indicators point to NGC 5548 having a total reddening (Galactic + internal) of  $E(B - V) \approx 0.26 \pm 0.02$ , which is some fifteen times the Galactic reddening alone.
- (4) The unreddened spectral energy distribution of the continuum from the optical to  $\approx \lambda 1200$  is consistent with the expected  $F_\nu \propto \nu^{+1/3}$  of an externally-illuminated accretion disc.
- (5) The velocity-integrated flux ratios of the broad hydrogen lines are close to Case B values.
- (6) A steep SMC-like reddening curve is ruled out for NGC 5548.
- (7) If the reddening of NGC 5548 is  $E(B - V) = 0.26$ , this gives an extinction in the V band,  $A_V = 0.8$  magnitudes, which is attenuation of just over a factor of two.
- (8) The UV luminosity of NGC 5548 around  $\lambda 1200$  has been underestimated by a factor of  $\approx 7$ . This value only depends weakly on the choice of reddening curve.
- (9) The higher luminosity predicts an accretion disc size that is  $\approx 2.6$  times larger than would otherwise be predicted. This solves the “accretion disc size problem”.
- (10) Higher luminosities in the far UV explain the higher IR emission in reddened AGNs.
- (11) Because radiation absorbed in the optical to far UV must be re-radiated in the IR, the contribution of AGN heating to the mid-IR emission of an AGN is greater than has been thought and the contribution of heating by hot stars correspondingly less.
- (12) Eddington ratios are higher and this helps reconcile AGN counts with local black hole demographics (the Sołtan argument).

## ACKNOWLEDGMENTS

FCA, SAB and SG carried out their work under the auspices of the Science Internship Program (SIP) of the University of California at Santa Cruz. We wish to express our appreciation to Raja GuhaThakurta for his excellent leadership of the program. MG is grateful to Ski Antonucci and Clio Heard for useful discussions.

## DATA AVAILABILITY

Data from the *International AGN Watch* monitoring campaigns are available at <https://www.asc.ohio-state.edu/astronomy/agnwatch/data.html>. Other data are available in the references cited.

## REFERENCES

- Antonucci, R. R. J. 2012, *Astron. & Astrophys. Trans.*, 27, 557
- Baker J. G., Menzel D. H., Aller L. H., 1938, *ApJ*, 88, 422. doi:10.1086/143997
- Baldwin, J. A., Ferland, G. J., Korista, K. T., et al. 1996, *ApJ*, 461, 664
- Bechtold, J., Shields, J., Rieke, M., et al. 1997, *IAU Colloq. 159: Emission Lines in Active Galaxies: New Methods and Techniques*, 113, 122
- Bentz, M. C., Denney, K. D., Grier, C. J., et al. 2013, *ApJ*, 767, 149
- Bottorff, M. C., Baldwin, J. A., Ferland, G. J., Ferguson, J. W., & Korista, K. T. 2002, *ApJ*, 581, 932
- Cackett E. M., Horne K., Winkler H., 2007, *MNRAS*, 380, 669. doi:10.1111/j.1365-2966.2007.12098.x
- Carleton, N. P., Elvis, M., Fabbiano, G., et al. 1987, *ApJ*, 318, 595
- Chamberlain J. W., 1953, *ApJ*, 117, 387. doi:10.1086/145704
- Chołoniewski, J. 1981, *Act. Astron. Ap.*, 31, 293
- Clavel, J., et al. 1991, *ApJ*, 366, 64
- Crenshaw, D. M. 1986, *ApJS*, 62, 821
- Czerny, B., Li, J., Loska, Z., & Szczerba, R. 2004, *MNRAS*, 348, L54
- De Rosa G., Peterson B. M., Ely J., Kriss G. A., Crenshaw D. M., Horne K., Korista K. T., et al., 2015, *ApJ*, 806, 128. doi:10.1088/0004-637X/806/1/128
- De Rosa G., Fausnaugh M. M., Grier C. J., Peterson B. M., Denney K. D., Horne K., Bentz M. C., et al., 2018, *ApJ*, 866, 133. doi:10.3847/1538-4357/aadd11
- Dibai, E. A. 1977, *Soviet Astron. Lett.*, 3, 1
- Dietrich M., Kollatschny W., Peterson B. M., Bechtold J., Bertram R., Bochkarev N. G., Boroson T. A., et al., 1993, *ApJ*, 408, 416. doi:10.1086/172599
- Dietrich, M., Bender, C. F., Bergmann, D. J., et al. 2001, *A&Ap*, 371, 79
- Edelson R., Gelbord J. M., Horne K., McHardy I. M., Peterson B. M., Arévalo P., Breeveld A. A., et al., 2015, *ApJ*, 806, 129. doi:10.1088/0004-637X/806/1/129
- Fausnaugh M. M., Denney K. D., Barth A. J., Bentz M. C., Bottorff M. C., Carini M. T., Croxall K. V., et al., 2016, *ApJ*, 821, 56. doi:10.3847/0004-637X/821/1/56
- Ferland G. J., 1999, *PASP*, 111, 1524. doi:10.1086/316466
- Ferland G. J., Shields G. A., 1985, in *Astrophysics of active galaxies and quasi-stellar objects* (Mill Valley, CA, University Science Books), pp. 157-184.
- Friedjung, M. 1985, *A&Ap*, 146, 366
- Gaskell, C. M. 1982, *PASP*, 94, 891
- Gaskell, C. M. 1984, *ApLett*, 24, 43
- Gaskell C. M., 2007, *ASPC*, 373, 596
- Gaskell, C. M. 2009, *New Astron. Rev*, 53, 140
- Gaskell, C. M. 2008, *Revista Mexicana de Astron. y Astrofis. Conf. Ser.*, 32, 1
- Gaskell, C. M., 2017, *MNRAS*, 467, 226. doi:10.1093/mnras/stx094
- Gaskell C. M., Bartel K., Deffner J. N., Xia I., 2021, *MNRAS*, 508, 6077. doi:10.1093/mnras/stab2443
- Gaskell, C. M., & Benker, A. J. 2007, arXiv:0711.1013
- Gaskell C. M., Gill J. J. M., Singh J., 2016, arXiv, arXiv:1611.03733

- Gaskell, C. M., Goosmann, R. W., Antonucci, R. R. J., & Whysong, D. H. 2004, *ApJ*, 616, 147
- Gaskell C. M., Harrington P. Z., 2018, *MNRAS*, 478, 1660. doi:10.1093/mnras/sty848
- Gaskell, C. M., Klimek, E. S., & Nazarova, L. S. 2007, *ApJ*, submitted [arXiv:0711.1025]
- Gaskell M., Thakur N., Tian B., Saravanan A., 2022, *AN*, 343, e210112. doi:10.1002/asna.20210112
- Goodrich R. W., 1989, *ApJ*, 340, 190. doi:10.1086/167384
- Grandi, S. A. 1980, *ApJ*, 238, 10
- Grandi, S. A. 1983, *ApJ*, 268, 591
- Heard C. Z. P., Gaskell C. M., 2022, *MNRAS* in press. doi:10.1093/mnras/stac2220 [arXiv, arXiv:2108.09995]
- Isoke, T., Feigelson, E. D., Akritas, M. G., & Babu, G. J. 1990, *ApJ*, 364, 104
- Kaspi S., Smith P. S., Netzer H., Maoz D., Jannuzi B. T., Giveon U., 2000, *ApJ*, 533, 631. doi:10.1086/308704
- Kelly B. C., Vestergaard M., Fan X., Hopkins P., Hernquist L., Siemiginowska A., 2010, *ApJ*, 719, 1315. doi:10.1088/0004-637X/719/2/1315
- Kollmeier J. A., Onken C. A., Kochanek C. S., Gould A., Weinberg D. H., Dietrich M., Cool R., et al., 2006, *ApJ*, 648, 128. doi:10.1086/505646
- Koratkar A. P., Gaskell C. M., 1991, *ApJL*, 370, L61. doi:10.1086/185977
- Korista, K. T., et al. 1995, *ApJS*, 97, 285
- Kriss G. A., De Rosa G., Ely J., Peterson B. M., Kaastra J., Mehdipour M., Ferland G. J., et al., 2019, *ApJ*, 881, 153. doi:10.3847/1538-4357/ab3049
- Krolik J. H., Horne K., Kallman T. R., Malkan M. A., Edelson R. A., Kriss G. A., 1991, *ApJ*, 371, 541. doi:10.1086/169918
- Kwan, J., & Krolik, J. H. 1981, *ApJ*, 250, 478
- Landt, H., Bentz, M. C., Ward, M. J., et al. 2008, *ApJS*, 174, 282
- Lynden-Bell, D. 1969, *Nature*, 223, 690
- MacAlpine, G. M. 1981, *ApJ*, 251, 465
- MacAlpine G. M., 2003, *RMxAC*, 18, 63
- Marconi A., Risaliti G., Gilli R., Hunt L. K., Maiolino R., Salvati M., 2004, *MNRAS*, 351, 169. doi:10.1111/j.1365-2966.2004.07765.x
- Mathews, W. G., & Wampler, E. J. 1985, *PASP*, 97, 966
- Matsuoka, Y., Oyabu, S., Tsuzuki, Y., & Kawara, K. 2007, *ApJ*, 663, 781
- Mehdipour M., Kaastra J. S., Kriss G. A., Cappi M., Petrucci P.-O., Steenbrugge K. C., Arav N., et al., 2015, *A&A*, 575, A22. doi:10.1051/0004-6361/201425373
- Netzer, H., & Davidson, K. 1979, *MNRAS*, 187, 871
- Netzer, H., Brotherton, M. S., Wills, B. J., et al. 1995, *ApJ*, 448, 27
- Osterbrock, D. E. 1977, *ApJ*, 215, 733
- Osterbrock, D. E., & Ferland, G. J. 2006, *Astrophysics of Gaseous Nebulae and Active Galactic Nuclei*, 2nd. ed. by D.E. Osterbrock and G.J. Ferland. Sausalito, CA: University Science Books
- Padovani P., Rafanelli P., 1988, *A&A*, 205, 53
- Pei L., Fausnaugh M. M., Barth A. J., Peterson B. M., Bentz M. C., De Rosa G., Denney K. D., et al., 2017, *ApJ*, 837, 131. doi:10.3847/1538-4357/aa5eb1
- Peterson, B. M., Balonek, T. J., Barker, E. S., et al. 1991, *ApJ*, 368, 119
- Peterson, B. M., Alloin, D., Axon, D., et al. 1992, *ApJ*, 392, 470
- Pooley, D., Blackburne, J. A., Rappaport, S., Schechter, P. L., & Fong, W.-f. 2006, *ApJ*, 648, 67
- Pooley, D., Blackburne, J. A., Rappaport, S., & Schechter, P. L. 2007, *ApJ*, 661, 19
- Richards, G. T., Hall, P. B., Vanden Berk, D. E., et al. 2003, *AJ*, 126, 1131
- Rodríguez-Ardila, A., Viegas, S. M., Pastoriza, M. G., Prato, L., & Donzelli, C. J. 2002, *ApJ*, 572, 94
- Sakata, Y., Minezaki, T., Yoshii, Y., et al. 2010, *ApJ*, 711, 461
- Schlafly, E. F., & Finkbeiner, D. P. 2011, *ApJ*, 737, 103
- Schlegel, D. J., Finkbeiner, D. P., & Davis, M. 1998, *ApJ*, 500, 525
- Sergeev, S. G., Doroshenko, V. T., Golubinskiy, Yu. V., Merkulova, N. I., & Sergeeva, E. A. 2005, *ApJ*, 622, 129
- Shapovalova, A. I., Doroshenko, V. T., Bochkarev, N. G., et al. 2004, *A&Ap*, 422, 925
- Shuder, J. M. 1982, *ApJ*, 259, 48
- Shuder, J. M., & MacAlpine, G. M. 1979, *ApJ*, 230, 348
- Sołtan, A. 1982, *MNRAS*, 200, 115
- Wampler, E. J. 1967, *PASP*, 79, 210
- Wampler, E. J. 1968, *AJ*, 73, 855
- K. D., Vestergaard, M., & Davis, T. M. 2011, *ApJL*, 740, L49
- Weingartner, J. C., & Draine, B. T. 2001, *ApJ*, 548, 296
- Winkler, H. 1997, *MNRAS*, 292, 273
- Winkler, H., Glass, I. S., van Wyk, F., et al. 1992, *MNRAS*, 257, 659
- Wysota, A., & Gaskell, C. M. 1988, in *Active Galactic Nuclei*, ed. H. R. Miller & P. J. Wiita, *Lecture Notes in Physics*, 307, 79
- Zheng, W. 1992, *ApJ*, 385, 127